2021

High-Temperature Organic Rankine Cycle Utilizing Novel Scroll Expander and Pump

Junyan Ren
Purdue University, ren102@purdue.edu

Nishad G. Damle
Purdue University

Stephen Caskey
Air Squared Inc.

Bryce R. Shaffer
Air Squared Inc.

Davide Ziviani
Purdue University

See next page for additional authors

GENSET WASTE HEAT RECOVERY THROUGH AN ORGANIC RANKINE CYCLE

Junyan REN[(a)], Nishad G. DAMLE[(a)], Stephen CASKEY[(b)], Bryce R. SHAFFER[(b)], Davide ZIVIANI[(a)], Eckhard A. GROLL[(a)]

[(a)] Ray W. Herrick Laboratories, Purdue University
West Lafayette, 47907-2099, USA,
ren102@purdue.edu, damlen@purdue.edu, dziviani@purdue.edu, groll@purdue.edu

[(b)] AirSquared Inc.
510 Burbank St., Broomfield, CO 80020, USA,
s.caskey@airsquared.com, bryce@airsquared.com

Abstract

Organic Rankine Cycles (ORC) are widely employed to extracting work from different heat sources to improve the operational efficiency of thermal systems. High-temperature ORCs (> 250 – 300 °C) are still particularly challenging especially when hydrocarbons cannot be used as the working fluids. Generators for Small Electric and Thermal Systems (GENSETs) are one example of systems where ORCs can be used as a bottoming cycle. A 1 kWe ORC has been previously constructed to evaluate the feasibility of designing an ORC with a heat source inlet temperature of approximately 500 °C. The test stand utilizes microtube evaporator, an air-cooled microchannel condenser, a plate heat exchanger as regenerator, scroll rotating machines as both expander and pump. To increase the efficiency of the ORC, novel scroll pump design and Oldham Ring scroll expander were installed. An extensive experimental campaign was carried out to map the performance of the expander and the pump along with the overall system performance using R245fa as the working fluid. In addition, thermocouple mesh has been inserted at the upstream and downstream of the evaporator to study the temperature maldistribution from the heat source. The performance was mapped at steady state over a range of operating conditions. The mapped performance has been used to develop a charge-sensitive dynamic model of the ORC system to be predict performance at off-design conditions and develop a control strategy. A discussion on the degradation of the lubricant oil in the system has also been included.

Introduction

Pairing up an Internal Combustion Engine (ICE) with an ORC system is concluded as one of the reasonable and simple approaches in recovering the waste heat during the combustion process [1]. With this technology emerging in the 1970s, research back then have realized a power output of 13% by introducing an ORC in ICE-WHR [2][3][4]. Nowadays, Cummins's "Super Truck" project in 2014 also reported a brake efficiency increase of 2.5% by introducing such technology [5]. WHR system from a ship engine coolant jacket is able to output 125 kWe from low grade thermal waste heat at 80-95 °C [6]. Another study also evaluates the ORC performance of an ORC WHR system from batch, gas-fired coffee roasting [7]. Chatsopoulou et al. concluded more power advantages can be seen when using plate heat exchangers and piston expanders in an ORC, under off-design conditions in an ICE. It was also concluded that the performance of such systems is closely related to the heat exchanger type, and the expander type [8]

The expander plays an important role within an ORC system as one of the key components. With it generally being categorized into two main types: the dynamic expanding machines – such as axial turbine expanders, and the volumetric expanding machines – such as scroll expanders. [9]. With the latter type attracting more and more research to be conducted, studies have investigated its performance resulting from various types of compression machines [10]. Emhardt et al. [11] also investigated and concluded the relationships between an expander performance and the scroll geometries.

While using volumetric expanders in low to medium power (up to 500 kW) ORC systems is widely accepted due to the compactness and simplicity offered by such machines [12], employing scroll expanders in ORC systems also sees many challenges. For an oil-free 5 kW scroll expander, large torque fluctuations can be seen in CFD simulation for the expander operation [13]. Suman concluded that the large fluctuations are due to the wrap configuration and could be minimized through redesigning the expander. In terms of efficiencies during operation, promising purpose-built

scroll expander prototypes are only exhibiting a volumetric efficiency of 35% [14], in which large amounts of flow leakage at lower expander speeds were monitored, and the expander performance is hence significantly reduced. Similarly, CFD analysis with a 10 kWe scroll expander also provides insights in the leakages in radial and axial flows through the scrolls [15], but the radial leakages were greatly reduced at higher expander rotational velocities. As a result, a deeper look into the performances of prototype scroll expanders are needed.

The main objective with this research, is to further investigate the cycle performances for a 1 kWe ORC system utilizing R245fa as the working fluid, while also characterizing the performances for prototype expander and pump models provided by the project sponsor. The general form of this research project will follow performance characterization completed by Ziviani et al. on a 5 kWe, oil-free open-drive scroll expander [16].

With this idea, experimental work on a 1 kWe ORC unit was carried out, with experimental components selected after simulation results given in the modeling phase. The experiments carried out also targeted at parameterizing performance data on the novel scroll thermal expander and the scroll pump. Test matrices were generated on data collecting schemes, and experimental results were wrapped together during the data analysis phase. With the data successfully justifying and concluding the performance data of the pump and the expander, a few observations on the system setup itself were also evaluated. A summary of the experimental results is shown in Table 1.

Table 1. Summary of experimental test results

Maximum Expander Pressure Ratio (-)	5.928
Maximum Pump Pressure Ratio (-)	7.052
Highest Expander Isentropic Efficiency (-)	0.609
Highest Expander Power Output (kW)	1.111

1. Experimental Setup

1.1 System Modeling and Sizing

This research represents a proof of concept with the novel scroll expander and scroll pump integrated in an ORC system, along with their performance characterizations. The prototype expander and pump are placed between the high and low pressures of the vapor and liquid side of the system, respectively. Both devices are fixed volume ratio machines. The cycle also includes a regenerator, aiming to improve the efficiency of the cycle. A schematic of the experimental system and the initial simulation results of the cycle state points indicated in a T-s diagram are shown in Figure 1. With the specifications for the main components, such as heat exchangers, pump, and expander determined from the initial cycle modeling process, the test setup was constructed by utilizing an existing frame and some other resources from an older experiment available at the Herrick Laboratories. The photo of the test stand is shown in Figure 2.

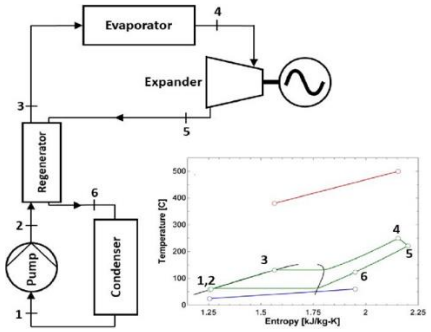

Figure 1. ORC Architecture [11]

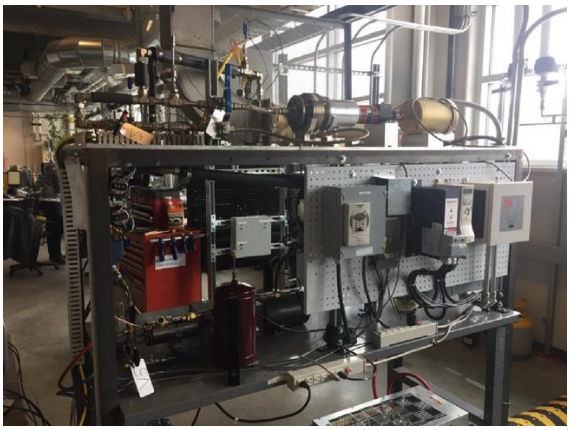

Figure 2. Experimental ORC Test Stand with Controllers on the Side Panel [11]

To determine the performance of the system and size its components, a simulation model of the system was created in EES [18]. EES is a versatile computational tool that was used to simulate different exhaust heat conditions of the internal combustion engine at different system operating conditions. A floating-point model was implemented, the inputs to this model were the heat sink parameters, such as the ambient temperature, condenser fan speed, condenser efficiency, low-side pressure, pump and expander efficiencies, expander fill factor, refrigerant mass flow rate, and regenerator pinch point. These parameters are used to guess the first state of the cycle after which the cycle progresses to calculate the states after pumping. This is done by modelling the pump through the basis of an isentropic efficiency and input parameters like refrigerant mass flow rate. The model then calculates that state after the high-pressure side of the regenerator. The state after the evaporation of the refrigerant was calculated by implementing a Jacobi point by point discretization of the evaporator to implement a two-dimensional heat exchange model and solve for the temperatures at different points in the heat exchanger. The expansion of the refrigerant in the scroll expander was calculated by using a semi-empirical expander model that accounts for the over or under expansion processes the flow then progresses going through the low-pressure side regenerator, here the heat transfer from the actual calculation is compared to that from the guess values and if required the guess values are updated for the process to converge. After the regeneration process the state 1 is calculated from the condensation process. This state 1 value is compared to the initial guess value for the state 1, once the criteria converge, the model calculates the overall power output of the system along with system performance parameters like cycle efficiency, pump efficiency, expander efficiency. This model was used to predict the sizing of the actual experimental setup by using the physical parameters of the actual components to predict the performance of the system.

1.2 Experimental Instabilities

The objective of the experimental activities was to map the performance data for the expander and the pump under controlled operating conditions. Measurements made throughout the 2018 to 2019 period were poorly documented, lacking clear and consistent parametric tables etc. etc., necessitating that this data be recollected to ensure final model quality. Throughout this recollection of data experimental instabilities were noted in the data, as visualized in Figure 4 showing the inlet temperature to the expander, in the test conditions outlined in Table 2 below.

Table 2: Experimental Instability Conditions

Expander Speed (RPM)	Pump Speed when Instability Occurred (RPM)
1200	2100
1800	2400
2400	2700
3000	2700
3600	N/A

The column on the right displays the pump speed when the instability first occurred where increasing the pump speed will still result in instable measurements. The instability was not observed at expander speed of 3600 RPM. All steady – state data collections were completed up until the expander inlet pressure reaches its limit of 28 bar.

The pattern shown in Figure 4 was taken at constant operating conditions: constant heat source temperature at 453 °C and flow rate of 76 CFM, constant pump speed at 2400 RPM, constant expander speed at 3000 RPM and constant heat sink temperature at 23.4 °C. Similar fluctuations are also shown in the measured mass flow rate plotted in Figure 4. The maximum fluctuations can be seen near 700 s and 1400 s, with backflow indicated by the negative flow rate which corresponds to the "peaks" on the temperature measurement in Figure 3. It was considered that two-phase flow is occurring at these times and a literature review was conducted to investigate this flow pattern.

Observations were made by Liu et al. [17] on slug flow in microchannel heat exchangers (MCHEs). They stated that when the MCHE inlet is at the liquid-vapor mixture state of the working fluid, bubbles within the microchannels can be seen. This assumption was then successfully observed in their experiments and matches the plotted results of their CFD simulation. The observed data and the CFD results are plotted in Figure 5. Further diving into their simulation, the resulting behavior within temperature measurements can then be seen in Figure 6.

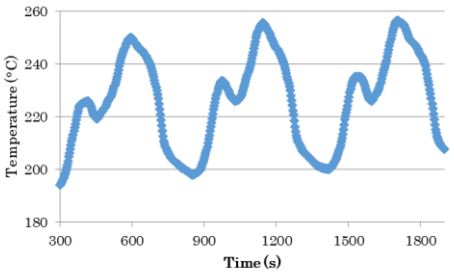

Figure 3. Experimental fluctuations of the expander inlet temperature.

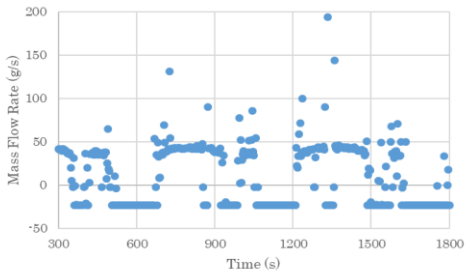

Figure 4. Experimental fluctuations of the pump inlet mass flow rate.

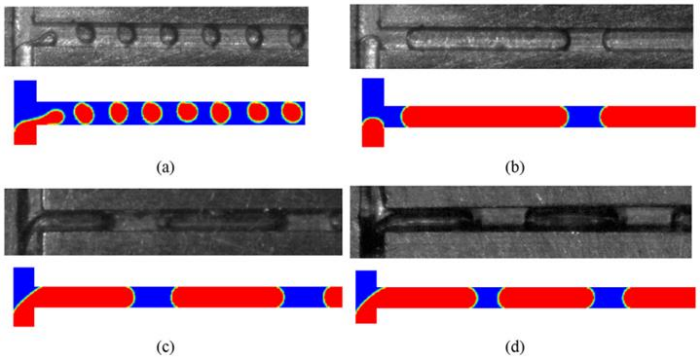

Figure 5. Flow patterns observed from experiment and CFD simulation. (a) QL = 4.32 mL/min, QG = 2.16 mL/min, H = 300 μm. (b) QL = 0.135 mL/min, QG = 0.54 mL/min, H = 300 μm. (c) QL = 1.62 mL/min, QG = 3.24 mL/min, H = 600 μm. (d) QL = 6.48 mL/min, QG = 3.24 mL/min, H = 900 μm. [17]

Additionally, Chang *et al.* [19] also investigated slug flow through microchannels and concluded that the cyclic pattern might be caused by the observed reversed flow inside the microchannels. It was believed that the fluctuations seen in Figures 3 and 4 were a result of intermittent two phase or slug flows. However, with the available experimental setup, project focus, and timeline, physically investigating this phenomenon is considered outside the project scope.

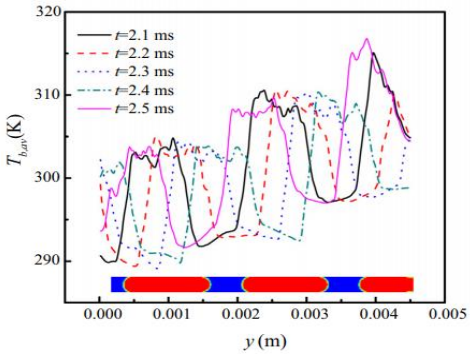

Figure 6. Temperature distribution of the fluid at different time along the flow direction (blue is liquid and red is gas) for case $\dot{V}_L$ = 0.54 mL/min, $\dot{V}_G$ = 1.08 mL/min, q_w = 10 kW/m^2. [19]

2. Experimental Testing

2.1 Test Matrix and Data Processing

The objective of the experimental setup is to characterize the performance of the pump and expander within the ORC.

The measurements were carried out with exhaust temperature measurements, and the data was documented to show any changes made to the system. For example, the charge level in the system is recorded each time.

Table 3: Test Matrix

Test	Expander Speed (RPM)	Pump Speed Maximum Range (RPM)
#1	1200	720 ~ 3600
#2	1800	
#3	2400	
#4	3000	
#5	3600	

The general test matrix for the experiment measurements are listed in Table 3 The mapping data for the expander was characterized at various pre-determined fixed-speed levels, as shown in the Expander Speed column in Table 3. The mapping process was completed by fixing the expander speed and varying the pump speed. The lower threshold was characterized by rotational speed that guarantees the lowest flow rate inside the system of approximately 5 g/s. The upper threshold was determined by the dynamic system parameters while the maximum limit stated by the manufacturer is 3600 RPM. Whether the expander inlet superheat the pump inlet subcooling can be maintained at pre-determined values or not. These values are approximately 100 K for expander superheat and less than 3 K for pump subcooling. Furthermore, the upper threshold was also determined by observing whether the system exhibits cyclic fluctuation behavior, which will be elaborated upon in this report. The mapping points were obtained at pre-determined steady-state conditions, the criteria for which are indicated in Table 4.

Table 4: Steady State Criteria

Measurement	Steady State Criteria
Temperature	Abs. difference < 0.5 K
Pressure	Change < 2%
Mass Flow Rate	Change < 2%
Rotational Speed	Change < 2%

When analyzing the results, the gravitational potential energy of the working fluid, the mechanical loss through the pump and expander motors, and the heat loss to the environment were all assumed to be negligible. With consideration of these assumptions, the theoretical fluid power can be calculated from Equation 1.

$$\dot{W}_{Exp} = \dot{m}(h_{Exp_{in}} - h_{Exp_{out}}) \quad (1)$$

while the actual power output is measured through a rotary torque sensor coupled to the shaft of the expander, where the mechanical losses are assumed to be negligible.

The theory of higher speeds corresponding to higher performances also lies in the filling factor (FF) of the expander, which can be calculated from Equation 2 [12]:

$$FF_{Exp} = \frac{\dot{V}_{Flow}}{f * V_{Exp}} \quad (2)$$

where f is the expander speed frequency and V_{Exp} is the displacement volume inside the expander. The FF acts as a representation of effective flow throughout the expander. An FF close to unity signifies nearly all flow is contributing to work production through the expansion process, A larger FF (FF > 1) represents leakage exists in the form of excessive flow inside the expansion chamber. An FF below unity would suggest that the expansion chamber is not completely filled with the working fluid.

Finally, the isentropic efficiency of the expander is calculated by:

$$\eta_{Exp} = \frac{\dot{W}_{Exp}}{\dot{m}(h_{Exp_{in}} - h_{Exp_{out.s}})} \quad (3)$$

2.2 Experimental Results

With the measurement completed at steady-state conditions, the measured performance of the expander and the pump is then input into EES [18] and plotted for different operating conditions. Higher pump speeds tend to push more flow through the system, and result in an overall trend of higher efficiency and power output. System behavior such as leakages at maximum conditions can also be observed at high pressure ratios across the expander, which will be Figure 7. Overall, an optimum can be observed in the plotted data points, where the higher expander speeds correspond to higher expander performance.

The maximum isentropic efficiency of approximately 0.61 occurred at pressure ratio (r_p) of 4.03 with a system charge of 15 lbs, and an expander speed of 3600 RPM. The performance data of the expander is plotted with respect to expander pressure ratio in Figure 7, Figure 8 and Figure 9.

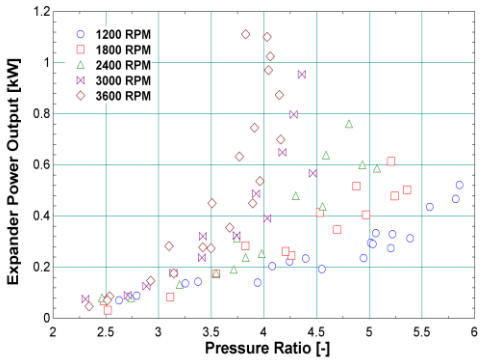

Figure 7: Expander power output vs. pressure ratio at different expander speeds

The expander exhibits an optimum power generation capability at r_p = 3.8 with 1.1 kWe of power. This condition is achieved by a mass flow rate at 52.41 g/s and a heat source temperature at 513.84 °C. With the expander shaft speed decreasing, the measured performance observed at different test conditions tend to occupy a wider range of pressure ratios, and with the lowest speed tested at 1200 RPM, the data covers the widest range of pressure ratios from 2.5 to

5.8. This range is 42.4% wider than that at 3600 RPM, while the average power generated at 1200 RPM is 50.7% lower than that at 3600 RPM. Leakage at maximum speed in the expander can be observed from the top four datapoints in Figure 7 at 3600 RPM, where the power output continues to increase despite the pressure ratio across the expander is falling with increasing gradient. In fact, the calculated filling factor throughout the four points has increased from 1.49 to 1.51 – signifying more leakage exists within the expansion chamber.

The isentropic efficiency of the expander displays a smoother behavior at optimum performances. Comparing to the leakages displayed by the top four points in Figure 7, the points in Figure 8 exhibits a rather saturated pattern. It can be concluded that the expander is displaying its optimum performance at these data points, or operating conditions; however, with the pump speed increasing, the expansion chamber is not capable of consisting more flow per revolution, the isentropic efficiency remains saturated at maximum value, while a slight increase in power generation is observed.

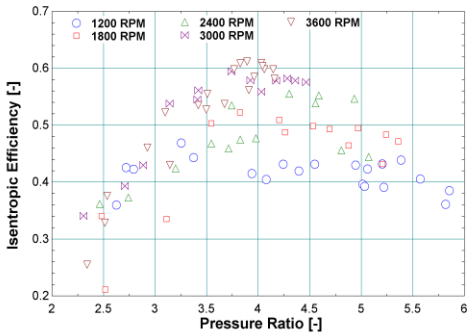

Figure 8: Expander isentropic efficiency vs. pressure ratio, at different expander speeds

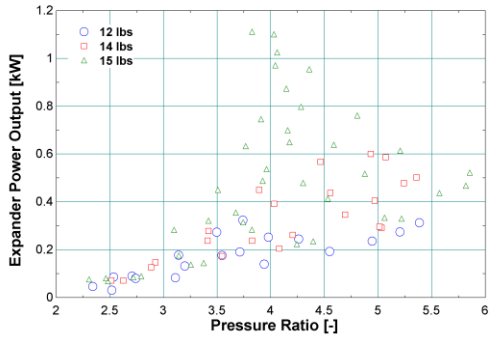

Figure 9: Expander power output vs. pressure ratio, at different charge levels

With the vertical axis being power output, the same behavior can be seen in Figure 9 comparing to Figure 7 . Higher performance can be seen correlating to higher charge levels in the system. As more mass is moved around the system, more mass then contributes to power generation inside the expansion chamber, with Equation (1), the theoretical expected power from the expander then increases. Furthermore, with the system being charged with more working fluid, a higher pressure ratio can therefore be achieved. This can also be observed by comparing data points at 15 lbs and 12 lbs in Figure 9.

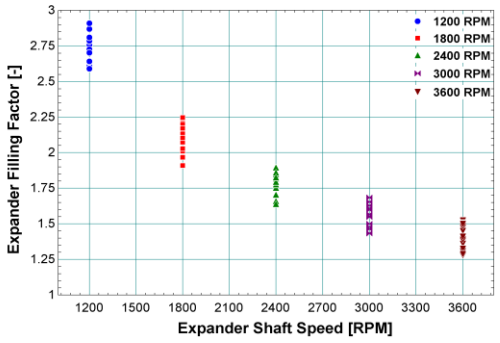

Figure 10: Expander filling factor vs. expander shaft rotational speed

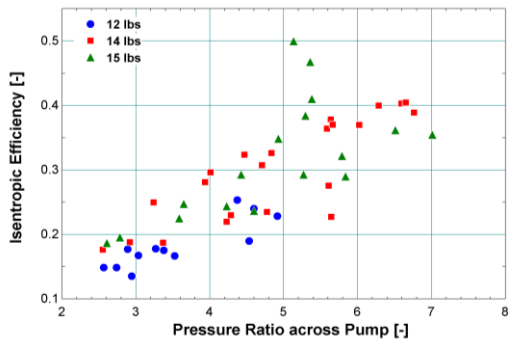

Figure 11: Pump isentropic efficiency performance plot, at different charge levels

With the power generated at 1200 RPM being 50.7% lower than that at 3600 RPM, the average filling factor at 1200 RPM results in being 52.5% higher than that at 3600 RPM. This further concludes that the expander performance is closely related to its filling factor. By operating the expander at higher shaft speeds, the amount of leakage in the expansion chamber is effectively reduced, hence result in a filling factor smaller in magnitude, and the capability of reaching higher performances. This also agrees with the trends observed in Figure 7, Figure 8 and Figure 9.

The performance data for the pump is plotted in Figure 11. The general trend for the pump performance is simliar to the expander, with increased pressure ratios being achieved with higher charge levels. While the higher pressure ratios corresponding to a higher isentropic efficiency is also similar to the expander performance, a decrease in the pressure ratio with an increase in the isentropic efficiency can be seen within a few datapoints at 15 lbs in Figure 12. It is believed that, with the amount of charge in the system and the particular test conditions at those data points, there is already an excessive amount of fluid being fed into the pump. This results in a larger mass flow rate inside the system than the pump can handle, resulting in it reaching its maximum volumetric capacity. This can be observed with the pressure ratio peaked at around 5.4 at the top four points with the highest isentropic efficiencies. Similar behaviors can be seen in Figure 7 and Figure 9, where the pressure ratio across the scroll machine exhibits a negative trend once a certain pressure ratio was reached.

2.3 Cycle Performance

With the successful operation of the prototype expander and pump, the system performance was characterized. Maximum pressure ratios of 5.9 and 7.0 across the expander and pump, respectively, were observed. It is believed that the main cause for the discrepancy between these values is from the pressure drop through the heat exchangers and system tubing. On the hot side of the heat exchanger, there is a brazed plate internal regenerator and a microchannel evaporator, whereas on the low side there is a microchannel condenser. It is believed that a measurable pressure drop occurs due to the flow path geometries inside the heat exchangers.

With the pump generating the necessary pressure lift inside the system, the prototype expander outputs 1.11 kWe of power successfully. This serves as proof for the concept of this 1 kWe expander design, and therefore the design can be scaled up and fit into applications with larger power expectations.

3. Dynamic System Modeling

3.1 Model Description

The objective of the modeling effort is to implement the mapped experimental performance data of the scroll expander into a modeled ORC. This model captures all the physical parameters of the experimental setup, including the heat exchanger geometries, source and sink conditions, and the expander displacement volume. Using this information, parametric studies operating on various operating conditions, heat exchanger geometries, and even different working fluids can be analyzed using both the system schematic outlined in Figure 12 and the given expander and pump prototype models. This modeling process is completed using the Dymola software utility.

The heat transfer calculations at the two air - to - refrigerant heat exchangers were based on a constant thermal diffusivity assumption of $\alpha = 2000\ mm^2/s$, which is provided as a standard algorithm within the Modelica library [20]. The heat exchanger geometric data was input to the model corresponding to the exact parameters of the equipment installed in the test setup. All modeling studies performed assumed that the pump operates with a constant isentropic efficiency of 0.40.

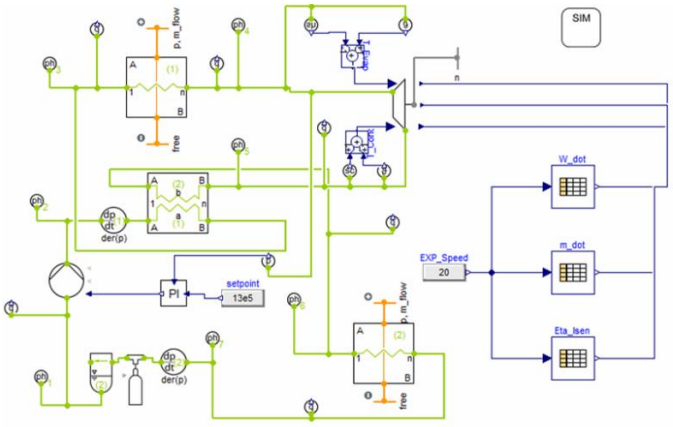

Figure 12. Dynamic ORC model in Modelica

3.1 Expander Mapping

The expander performance was mapped through polynomial coefficients, while the independent variables were set to the sink and source temperatures. Since the expander performance was characterized at different rotational speeds, the actual mapping process is also completed by assigning a polynomial, similar to that of Equation (4), to every speed level. As a result, the expander performance map consists of five polynomials corresponding to the five speed levels in the test matrix.

In order to implement the variable speed mapping data into the Dymola model, the mapped expander model was constructed using three supplementary models. The primary model sets up the expander solver, which runs through internal calculations based on the geometrical data given for the expander (e.g., displacement volume and rotational speed). The secondary model sets up the mapped polynomials and assigns the mapped data to the desired modeled output. This model also provides a speed selection criterion based on the speed input from the user, in which the correct set of polynomial coefficients are selected corresponding to the specified input value. The third model contains the actual polynomials and functions as the I/O model for the mapping coefficients. Using the designated speed input, the polynomial coefficients are then output from this model to the second model for the actual calculation involving the polynomial. In summary, when the user inputs the desired speed and target evaporating and condensing temperatures, the speed is processed in the second model, and fed into the third model along with the temperatures. Final modeled parameters are then output from the third model. The first model exists in order to make the remaining models function properly in the software.

In summary, the first model restricts the Dymola software to recognize the combined model as an expander model; the second model sets up the selection criteria where the third model contains the coefficients. When the user input the desired speed, the criteria in the second model feeds the speed into the third model, and the corresponding coefficients are then returned into the second model for outputting the final modeled parameters by also receiving the evaporation and condensing temperatures from the simulated system.

The implemented expander map follows a similar logic to the compressor map, whereby a multi-coefficient polynomial is generated as a curve of best fit for the experimental data. The general form of the equation is illustrated in the polynomial defined in Equation (4).

$$\dot{m}_{Map} = a_1 + a_2 * T_{Cond} + a_3 * T_{Cond}^2 + a_4 * T_{Cond}^3 + a_5 * T_{Evap} + a_6 * T_{Evap}^2 + a_7 * T_{Evap}^3 + a_8 * T_{Cond} * T_{Evap} + a_9 * T_{Evap}^2 * T_{Cond} + a_{10} * T_{Cond}^2 * T_{Evap} + a_{11} * T_{Cond}^2 * T_{Evap}^2 \quad (4)$$

Where a_n is the coefficient from the map, T_{Cond} is the condensing temperature, T_{Evap} is the evaporation temperature, and $\dot{m}_{Map}$ represents the mapped mass flow rate through the expander. All mapped polynomials show excellent agreement with the actual expander performance, which is supported by an average coefficient of determination R^2 score of 0.986.

4. Conclusions and Future Work

Following the completion of both expander and pump performance maps using experimental data, the primary objective of this project has been accomplished. Generally, a positive trend can be observed between the pressure ratio between the scroll devices and the expected performance (power output, isentropic efficiency, etc.). A power output of 1.1 kW is obtained at 15 lb, 3600 rpm of the expander, thus proving that the test model satisfactorily achieves the scaled target. Higher pressure ratios and rotational speeds also lead to a lower Fill Factor at the expander, signifying a more effective flow being transferred through the device. The lowest filling factor of 1.30 occurred approximately at 3600 rpm, and the highest filling factor of 2.75 occurred approximately at 1200 rpm.

Some caveats of the test setup are also indicated through noticeable trends observed in the experimental data. For example, the current setup lacks the ability for further investigation of the fluctuations witnessed in the data collection process for the expander performance, which are theorized to develop from microchannel slug flow (i.e., the decrease in pressure ratios while the performance is measured higher). To better comprehend the complete system performance, future investigations of these phenomena should be conducted.

Nomenclature

Symbols:

A	Area, m^2
V	Volume, m^3
T	Temperature, K
h	Specific enthalpy, kJ/kg
s	Specific Entropy, kJ/ (kg-K)
W	Power, kWe
FF	Expander Filling Factor
$\dot{m}$	Mass flow rate, kg/s

Greek Symbols:

η	Isentropic Efficiency
α	Thermal Diffusivity, mm^2/s

Subscripts:

Exp	Expander
Pump	Pump
Evap	Evaporation
Cond	Condensation

Acknowledgement

The research group would like to send the appreciation to ARPA – E as the primary sponsor for this project, to Air Squared Inc. for providing the opportunity for Purdue to participate in this project, for their continuous feedback and insights throughout the whole process, and for their supports over this 5 – year period time. The gratitude also goes to all the Herrick Labs faculties who contributed by building, troubleshooting the whole system, and all the ones who provided their opinions on the challenges that occurred.

References

[1] Shi L, G. S. (2018), A review of modified Organic Rankine cycles (ORCs) for internal combustion engine waste heat recovery (ICE-WHR). Renewable and Sustainable Energy Reviews 92, 95-110.

[2] Morgan D., P. P. (1973), Laboratory test results, low emission ranking-cycle engine with organic based working fluid and reciprocating expander for automobiles. Intersociety Energy Conversion Engineering Conference, 1973.

[3] P.S. Patel, E. D. (1976), Compounding the truck diesel engine with an organic Rankine-cycle system. Diesel Trucks

[4] Doyle. E., L. D. (1979), Installation of a diesel-Organic Rankine compound engine in a class 8 truck for a single-vehicle test. Soc Automot Eng Prepr

[5] Delgado O., N. L. (2014), The US SuperTruck program: Expediting the development of advanced heavy-duty vehicle efficiency technologies. The international Council on Clean Transportation

[6] Sellers, C. (2017). Field operation of a 125 kW ORC with ship engine jacket water. Energy Procedia 129, 495-502.

[7] Pantaleo A, F. J. (2017). Intermittent waste heat recovery: Investment profitability of ORC cogeneration for batch, gas-fired coffee roasting. Energy Procedia 129, 575-582.

[8] Qiu G, H.L. (2011), Expanders for micro-CHP systems with Organic Rankine Cycle, Applied Thermal Engineering 31, 3301-3307

[9] Song P, W. M. (2015), A Review of Scroll Expanders for Organic Rankine Cycle Systems, Applied Thermal Engineering 75, 54-64

[10] Emhardt S, G. T (2018), A Review of Scroll Expander Geometries and their Performance, Applied Thermal Enginering 141, 1020-1034

[11] Lavernia, A. C. (2018). Micro-Scale Waste Heat Recovery from Stationary Internal Combustion Engines by Sub-Critical Organic Rankine Cycle Utilizing Scroll Machinery. MSME Thesis, Purdue University.

[12] Lemort, V. Q. (2009). Testing and Modeling a Scroll Expander Integrated into an Organic Rankine Cycle. Applied Thermal Engineering, 3094-3102.

[13] Kosmadakis G, G. M. (2017), Development of Open-Drive Scroll Expander for an Organic Rankine Cycle (ORC) Engine and First Test Results, Energy Procedia 129, 371-378

[14] Suman A, R. S. (2017). Experimental and Numerical Characterization of an Oil-Free Scroll Expander. Energy Procedia 129, 403-410.

[15] Song P, Z. W. (2017). Unsteady Leakage Flow through Axial Clearance of an ORC Scroll Expander. Energy Procedia 129, 355-362.

[16] Ziviani D, N. J. (2018), Experimental and numerical analyses of a 5 kWe oil-free open-drive scroll expander for small-scale organic Rankine cycle (ORC) applications. Applied Energy 230, 1140-1156

[17] Dongren Liu, X. L. (2020). Experimental and numerical analysis on heat transfer performance of slug slow in rectangular microchannel. International Journal of Heat and Mass Transfer 147.

[18] Klein, S.A. (2019), EES-Engineering Equation Solver, Version 10.643, F-Chart Software, http://fchart.com

[19] K.H. Chang, C. P. (2007). Two-phase flow instability for boiling in a microchannel heat sink. International Journal of Heat and Mass Transfer 50, 2078-2088.

[20] Dassault Systemes (2019), Dymola, https://www.3ds.com/products-services/catia/products/dymola/